THE JOURNAL OF PHYSICAL CHEMISTRY C
A JOURNAL OF THE AMERICAN CHEMICAL SOCIETY

pubs.acs.org/JPCC

Article

Hydrogen Interaction with Oxide Supports in the Presence and Absence of Platinum

Arik Beck,* Przemyslaw Rzepka, Kenneth P. Marshall, Dragos Stoian, Marc G. Willinger, and Jeroen A. van Bokhoven*

Cite This: J. Phys. Chem. C 2022, 126, 17589−17597

Read Online

ACCESS | Metrics & More | Article Recommendations | Supporting Information

ABSTRACT: Oxides are essential catalysts and supports for noble metal catalysts. Their interaction with hydrogen enables, e.g., their use as a hydrogenation catalyst. Among the oxides considered reducible, substantial differences exist in their capability to activate hydrogen and how the oxide structure transforms due to this interaction. Noble metals, like platinum, generally enhance the oxide reduction by hydrogen spillover. This work presents a systematic temperature-programmed reduction study (300 to 873 K) of iron oxide, ceria, titania, zirconia, and alumina, with and without supported platinum. For all catalysts, platinum enhances the reducibility of the oxide. However, there are pronounced differences among all catalysts.

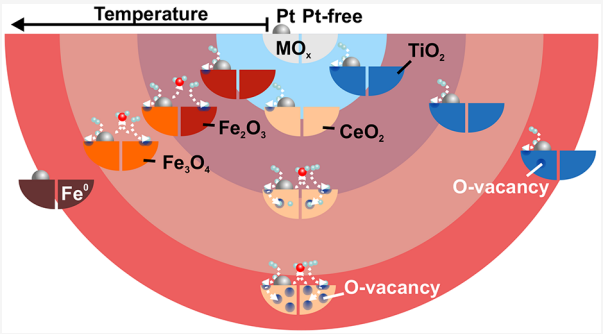

INTRODUCTION

Heterogeneous catalysis is the backbone of the modern chemical industry. Among the materials frequently used for catalysis are transition metal oxides, either as catalysts[1] or as supports for nanosized metals.[2] In the latter case, the metal oxide support is not a mere active site carrier but adds essential functions by so-called metal−support interactions.[3] Such catalysts are often exposed to hydrogen atmospheres during the activation procedure to transform the catalyst precursor into an active state,[4] e.g., by reduction of the supported metal or to induce structural modifications,[5] or during the actual catalytic operation in (de)hydrogenation reactions.[6,7] Especially the use of oxides in catalyzed hydrogenation reactions is interesting. However, why some oxides act as better hydrogenation catalysts or supports than others is still poorly understood.[8] The activation of molecular hydrogen on the catalyst surface is critical. A high energy barrier generally hampers hydrogen activation on perfect metal oxide surfaces; e.g., hydrogen dissociation on iron oxide surfaces has an activation barrier of 4.4 eV.[9] In contrast, hydrogen dissociation on noble metals like platinum is barrier-free (<0.1 eV) and readily occurs below room temperature.[7,10−13] As a consequence, the presence of platinum on the metal oxide surface drastically influences the oxide by hydrogen spillover.[14,15] In the present study, we systematically investigated the hydrogen uptake behavior of iron(III) oxide, cerium(IV) oxide (ceria), zirconium(IV) oxide (zirconia), and aluminum(III) oxide (alumina) in the presence and absence of platinum. Platinum has, in all cases, an influence on the temperature of hydrogen uptake. However, the platinum-induced hydrogen uptake amount is oxide material dependent. In-situ X-ray diffraction of the two most reducible supports, iron oxide and ceria, revealed why some of the reported differences in catalytic performance among oxides, which are generally considered reducible, exist. This understanding, consequently, helps the decision process for suitable oxide catalysts and support materials.

METHODS AND MATERIALS

Sample Oreparation. Commercial iron(III) oxide (Pruratrem), cerium(IV) oxide (STREM Chemicals), titanium(IV) oxide Aeroxide P25 (Acros Organics (ACR), 26% rutile, 74% anatase), zirconium(IV) oxide (Acros Organics ACR), and γ-aluminum(III) oxide (Condea) were used as support material. The oxides were calcined in static air in a muffle furnace at 873 K for 12 h. After calcination, the support BET surface area was determined via nitrogen physisorption (Micromeritics Tristar). The platinum loading was adjusted to the determined surface area of the support to result in a constant platinum loading of around 3×10^{-4} $mmol_{Pt}$ m^{-2} (see Table 1). Electrostatic adsorption was used to deposit the platinum precursor (tetraammine platinum(II) nitrate (99.995%, Sigma-Aldrich)) on the oxides. The respective amount of precursor was dissolved in ultrapure water; the water amount was adjusted to the

Received: August 2, 2022
Revised: September 16, 2022
Published: October 10, 2022

Table 1. Platinum Loading and Surface Area of the Studied Oxide Materials

metal oxide	BET ($m^2\ g^{-1}$)	Pt loading (wt %)	Pt per surface unit (mmol m^{-2})
Fe_2O_3	7	0.045	3.4×10^{-4}
CeO_2	50	0.25	2.6×10^{-4}
TiO_2 (P25)	48	0.24	2.6×10^{-4}
ZrO_2	4	0.027	3.6×10^{-4}
γ-Al_2O_3	201	1.35	3.6×10^{-4}

support surface area (5000 $m^2\ L^{-1}$). Then the pH value of the solution was adjusted using ammonia to an initial pH value of 14. The oxide was added to the aqueous solution; the flask was covered; and the solution was stirred for 24 h. Then the cover was removed to evaporate water for 48 h. Finally, the materials were calcined at 623 K in static air for 1 h (heating ramp 5 K min^{-1}).

Temperature-Programmed Reduction (TPR). Reduction experiments in 10% H_2/Ar (Carbagas, >99.999% purity) at ambient pressure were performed with a Micromeritics AutoChem HP analyzer equipped with a temperature conductivity detector (TCD). For each experiment, the total gas flow was kept at 10 mL min^{-1}. During the analysis, the gas passed through a cold trap cooled with an ice-liquid slurry of isopropanol (184 K) to condense water produced by the reduction before the gas reached the TCD detector. For each experiment, around 60−100 mg of the material was loaded into a U-shaped quartz reactor tube. The sample was fixed between two quartz wool plugs. Before each TPR experiment, the sample was pretreated under a flow of He (50 mL min^{-1}) for 30 min at 373 K (ramp 20 K min^{-1}) to desorb loosely bound water from the sample surface. Subsequently, the sample was cooled to 263 K and equilibrated for 30 min. Then, the gas atmosphere was changed to 10% H_2/Ar, and the sample was exposed to that mixture for 30 min at 223 K. Then the TPR experiment was started, and the sample tube was heated to 873 K with a heating ramp of 10 K min^{-1}. At 873 K, the sample was kept for 20 min and then cooled to 303 K. The hydrogen uptake was measured during the complete heating and cooling cycle. Uptake refers to the difference between hydrogen content in the feed and outlet gas stream. The uptake can represent either incorporation into the catalyst or production of water.

In-Situ X-ray Powder Diffraction (XRD). In-situ XRD measurements were carried out at the BM31 beamline of the Swiss-Norwegian Beamlines (SNBL) at the European Synchrotron Research Facility (ESRF, Grenoble, France). The samples were presented in a flow capillary setup described by Chupas et al.[16] in a 0.7 mm inner diameter quartz capillary with 0.01 mm wall thickness (Hilgenberg). Around 5 mg of the sample was placed between quartz wool. The temperature was measured and controlled using a K-type thermocouple inside the capillary. The sample was heated using two ceramic-embedded tungsten coils. A gas mixture of Ar (>99.999% purity) and H_2 (>99.999% purity) was premixed to 50 mL min^{-1} containing 10% H_2. Initially, the sample was exposed to a flow of Ar for 5 min to remove air from the capillary; then, the gas feed was switched to the hydrogen mixture at 303 K. After another 5 min, the TPR experiment was started using a heating ramp of 5 K min^{-1}. The sample was heated to 873 K. When reaching the temperature, the sample was cooled to RT by turning the heaters off. Diffraction data were continuously collected at an X-ray beam energy of 36.6 keV in Debye−Scherrer geometry using the PerkinElmer Dexela 2923 CMOS detector.

X-ray Diffraction Pattern Refinement. The diffraction data were averaged every 50 scans. Before the Rietveld analysis, baselines were subtracted from all data sets using the program *Lines*.[17] The sequential refinement was performed using *TOPAS 7*.[18] The consecutive phases resulting from the initial phase reduction were simultaneously matched to all subsequent diffractograms, and their lattice parameters were refined. The profile of Bragg peaks and their instrumental broadening was described beforehand with the Pseudo−Voigt function defined in the data collected at LaB6 standard. The Lorentzian function was convoluted to the profile functions, and the integral breadth enabled deriving the crystallite size. Selected fits and data for Pt/CeO_2 (Figure S1) and Pt/Fe_2O_3 (Figure S2) are provided in the Supporting Information.

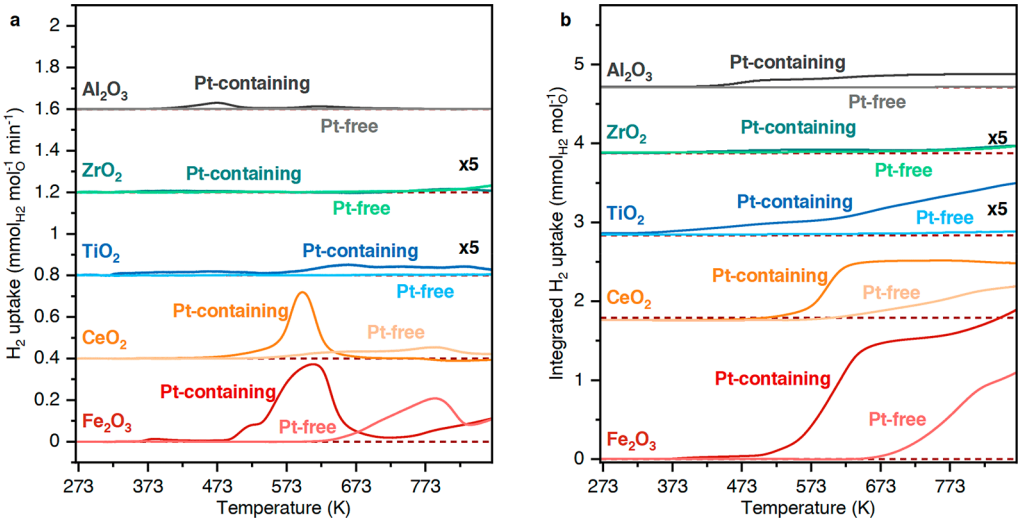

Figure 1. Temperature-dependent hydrogen uptake. (a) Temperature-programmed reduction (TPR) in 10% H_2/Ar (heating rate 10 K min^{-1}) of various metal oxides with and without platinum impregnation. The platinum weight loading was adjusted to the metal oxide surface area (see Table 1). (b) Accumulated hydrogen uptake during the TPR experiment. The label "x5" in (a) and (b) indicates that the data has been scaled 5-fold.

https://doi.org/10.1021/acs.jpcc.2c05478
J. Phys. Chem. C 2022, 126, 17589−17597

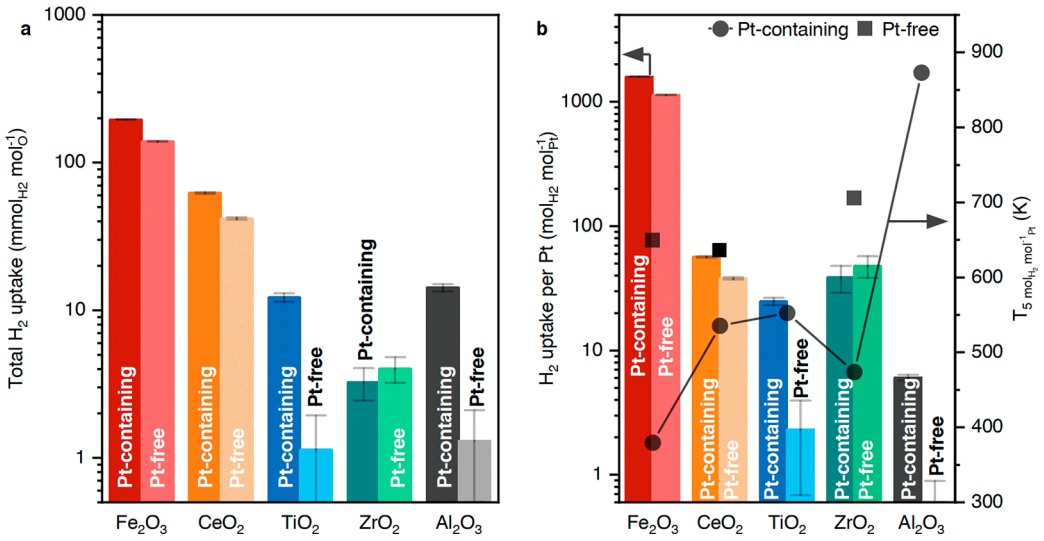

Figure 2. Oxide-dependent hydrogen uptake. (a) Total hydrogen uptake of the H_2-TPR experiment, including the heat up to 873 K, a dwell period of 30 min, and subsequent cool down to 298 K for the platinum-loaded and platinum-free samples. (b) Hydrogen uptake normalized to the platinum content of the samples, which also corresponds to a normalization per surface area. The Pt-free samples' normalization was performed using the same normalization factor per sample mass from the corresponding Pt-containing sample. Also, the temperature at which a total hydrogen uptake of 5 mol_{H2} mol^{-1}_{Pt} was reached for the platinum-loaded samples. For platinum-free titania and alumina this uptake amount was not reached within the experiment, and consequently, no data point is plotted for the two samples. The error bar was calculated based on the standard deviation of two performed TPR experiments.

RESULTS

This study considered five different oxide materials (Fe_2O_3, CeO_2, TiO_2, ZrO_2, and Al_2O_3). The oxides were chosen based on their different degrees of reducibility. In line with their decreasing reducibility, iron oxide, ceria, titania, zirconia, and alumina show an increasing band gap[19] (2.1, 3.0, 3.2, 5.4, and 7.3 eV). The oxides were impregnated with platinum. The concentration of platinum per surface area is decisive for the nature and size of formed platinum nanostructures.[20] Therefore, the platinum weight loading was adjusted for all catalysts to the measured BET area of the catalyst (Table 1), yielding a platinum surface concentration of 0.187 $atoms_{Pt}$ nm^{-2}.

Figure 1 shows the transient and accumulated hydrogen uptake[7,21] during the heating phase of the TPR for all oxides with and without platinum loading. Uptake can either occur by chemisorption of hydrogen in the sample or through water formation. Platinum-free iron oxide and ceria show pronounced hydrogen uptake starting at 603 and 585 K, respectively. However, the uptake process was not completed at the highest temperature for iron oxide. Titania and zirconia show limited hydrogen uptake. Lastly, alumina shows essentially no hydrogen uptake. The presence of platinum on these supports yielded an apparent change in the TPR behavior for all samples. In the presence of platinum, an additional uptake originates from the complete reduction of platinum oxide, formed by the calcination,[7] even though the platinum loading is low. Despite the low platinum loading of 0.045 wt % on the iron oxide surface, the principal reduction peak shifts by about 150 K to lower temperatures due to the presence of platinum, while the uptake is also incomplete at the end of the experiment. A similar shift and increase in total uptake are seen for the ceria sample (Figure 1b). For Pt/TiO_2, a detectable hydrogen uptake occurs, starting at low temperatures (360 K). Also, the TPR pattern of Pt/ZrO_2 shows a small uptake peak at low temperature; overall, however, the process appears to be not drastically different from platinum-free zirconia. The TPR pattern of the Pt/Al_2O_3 sample shows two uptake peaks, which have been absent in the platinum-free sample. The Pt/Al_2O_3 sample has the highest weight loading of 1.35 wt %, and the platinum oxide reduction is easily observable. These two peaks have therefore been assigned to the reduction of platinum oxide, which is firmly anchored on alumina surfaces.[21,22] The presence of two peaks potentially originates from the initial reduction of the oxidized platinum nanoparticles and later interfacial reduction.[23,24]

By this qualitative inspection, the hydrogen uptake differs for each oxide. Figure 2a shows the quantified hydrogen uptake of the TPR experiments. The hydrogen uptake was normalized to the theoretically calculated total amount of oxygen in the oxides. In the case of the platinum-loaded iron oxide, the hydrogen uptake of 195 $mmol_{H2}$ mol^{-1}_{O} corresponds to the removal of one-fifth of the total oxygen in the iron oxide. The total uptake is strongly oxide-dependent. Iron oxide has the highest uptake, and the presence of platinum increased the hydrogen uptake by 41%. Ceria had around three times smaller hydrogen uptake, and the presence of platinum increased the uptake by 47%. Titania presents an exceptional case: in the presence of platinum, the hydrogen uptake is around five times smaller than for ceria. However, this uptake is 1100% higher than for the platinum-free titania sample and starts to occur at temperatures around 300 K, the lowest temperature observed in this experimental series. The uptake for zirconia was 3.3 $mmol_{H2}$ mol^{-1}_{O} and 4.0 $mmol_{H2}$ mol^{-1}_{O} for the platinum-loaded and platinum-free catalysts. This was a low uptake. Consequently, the difference of 0.7 $mmol_{H2}$ mol^{-1}_{O} in the two experiments is within the experimental error. Lastly, the alumina samples show a hydrogen uptake comparable to that of titania.

Figure 2b shows the hydrogen uptake normalized to the amount of platinum, which also corresponds to a normalization per surface area. The normalized uptake for the platinum-free samples is also depicted using the same normalization factor as for the corresponding platinum-loaded sample. Comparing the

https://doi.org/10.1021/acs.jpcc.2c05478
J. Phys. Chem. C 2022, 126, 17589−17597

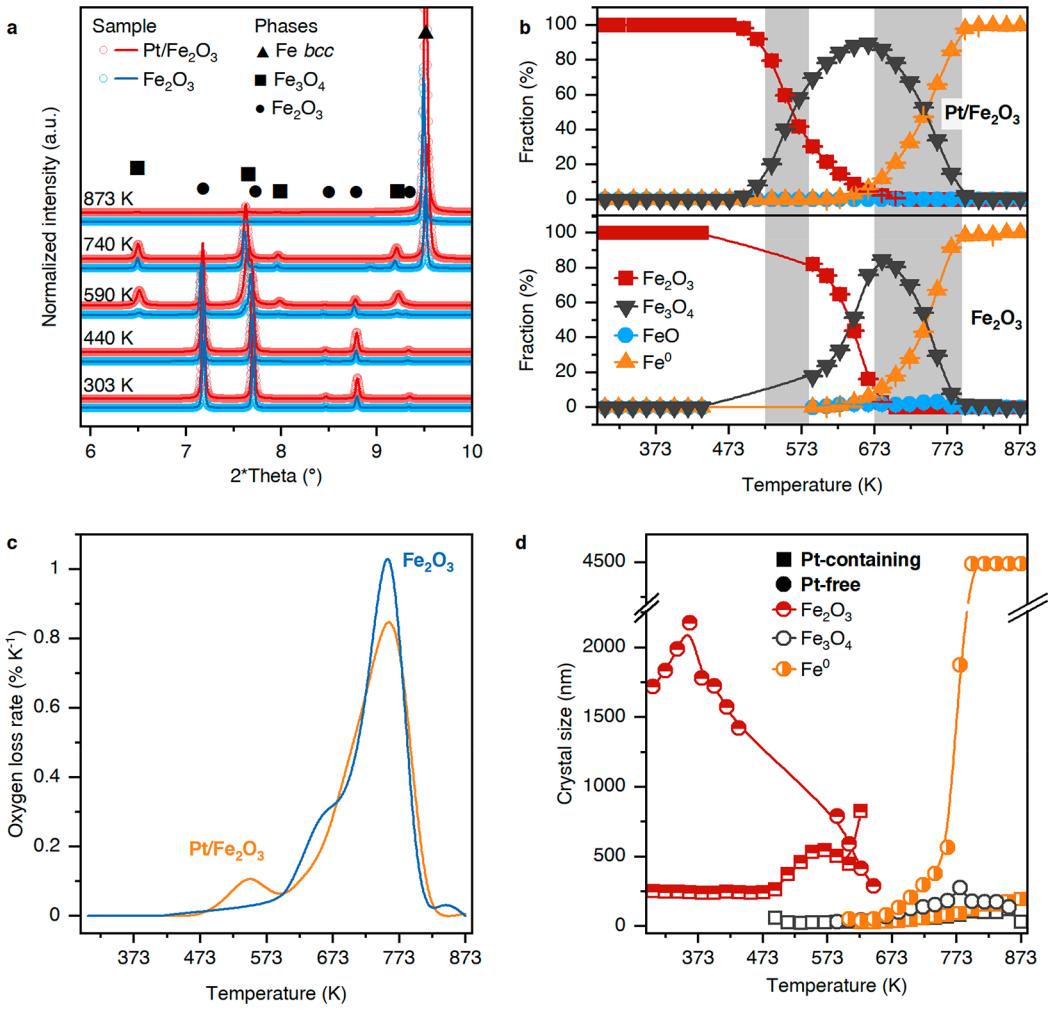

Figure 3. In-situ X-ray powder diffraction of iron oxide samples. In-situ XRD patterns recorded with 36.6 keV X-rays. TPR experiments were performed in 10% H_2/Ar and a heating ramp of 5 K min^{-1}. (a) Selected diffraction patterns of Pt/Fe_2O_3 and Fe_2O_3 as a function of temperature. The solid line represents the fit, and circle symbols are the data. (b) Weight fractions of crystalline Fe_2O_3, Fe_3O_4, FeO, and metallic Fe are determined by Rietveld refinement as a function of temperature (top panel: Pt/Fe_2O_3, bottom panel: Fe_2O_3). (c) Oxygen loss rate calculated by the first derivative of the oxygen content determined by the phase fractions depicted in (b). (d) The crystal size of the present iron oxide phases (with a phase fraction >5%) was determined by Rietveld refinement.

platinum-normalized samples, iron oxide shows an almost 2 orders of magnitude larger value than ceria, titania, and zirconia. Those three oxides have very similar platinum-normalized values. Alumina follows with the lowest value of around 5 mol_{H2} mol^{-1}_{Pt}, showing that the platinum alumina sample can barely consume more hydrogen than needed for the platinum oxide reduction. Figure 2b also depicts the temperature at which this hydrogen uptake per platinum was reached (so for alumina, this is 873 K). This temperature was chosen since it allows a fair comparison between the different oxides and represents the start of the reduction that exceeds mere platinum oxide and platinum−oxide interface reduction. For comparison, the temperature for the same amount of hydrogen consumption is also given for the platinum-free samples. For platinum-free titania and alumina, this degree of hydrogen consumption was not reached by the end of the experiment.

Figure 2 allows general observations: Iron oxide is the strongest responder to a hydrogen environment. Also, in the absence of platinum, the hydrogen consumption implied interaction with more than 10% of the oxygen in the oxide lattice. Such interaction can be the removal of lattice oxygen by water formation, resulting in oxygen vacancies, the formation of hydroxyls and hydrides, and or phase transformations (e.g., Fe_3O_4, FeO, or Fe(0)). Especially with the iron oxide's low surface area, the reduction goes beyond a surface reduction, but bulk processes are involved. Platinum enhances this process significantly by reducing the temperature necessary for the uptake process by 150 K. Ceria, titania, and zirconia show, normalized by platinum and surface area, comparable uptake values, which indicate that for these oxides the surface area is decisive for the uptake process. For titania (P25), platinum has to be present to trigger reduction. For ceria and zirconia, the presence of platinum significantly shifts the required temperatures to lower values. The total amount of hydrogen uptake on zirconia is hardly affected by platinum. This obseravtion is in line with other studies[25−27] and suggests that the amount of hydrogen that is consumed by the zirconia catalysts is purely dependent on the zirconia structure. However, the kinetic barriers to produce vacacines and activate hydrogen are influenced by platinum, in line with theory.[28,29]

https://doi.org/10.1021/acs.jpcc.2c05478
J. Phys. Chem. C 2022, 126, 17589−17597

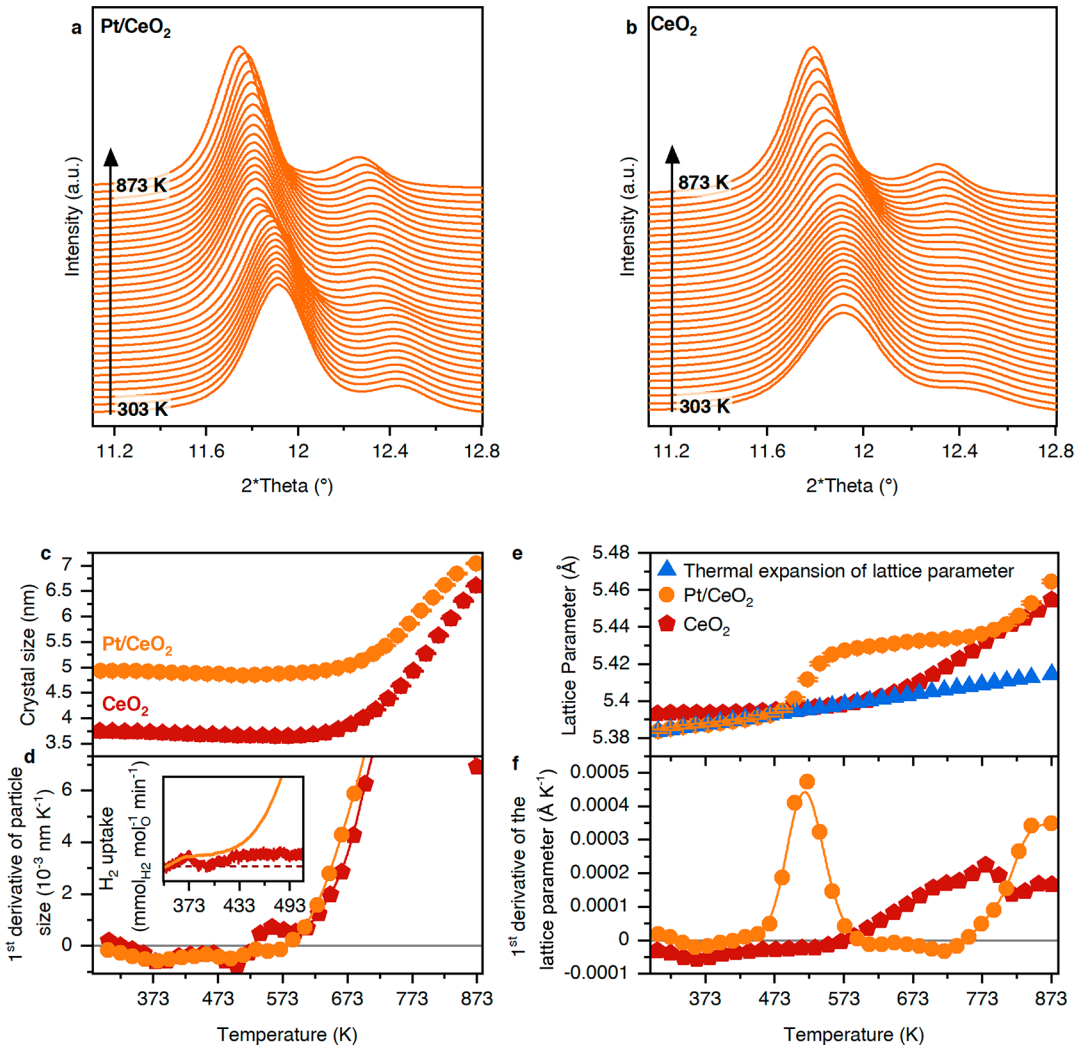

Figure 4. In-situ X-ray powder diffraction of ceria samples. In-situ XRD patterns recorded with 36.6 keV X-rays. TPR experiments were performed in 10% H_2/Ar and a heating ramp of 5 K min^{-1}. Diffraction patterns of (a) Pt/CeO_2 and (b) CeO_2 during the TPR experiment. (c) Evolution of the ceria particle size as a function of temperature. (d) The first derivative of the particle size of ceria. The particle size shows a negative evolution at low temperatures. These negative trends coincide with the onset of hydrogen uptake in the inset. (e) Change in the ceria lattice parameter and the expected lattice parameter change with temperature assuming a constant thermal expansion coefficient of $\alpha = 1 \times 10^{-5}$ K^{-1}.[40] The lattice parameter change originates from two contributions: thermal expansion and Ce^{3+} formation due to oxygen removal and hydrogen incorporation. (f) The first derivative of the measured lattice parameter corrected by the linear thermal expansion expected from the change in temperatures.

Pt/Al_2O_3, normalized by platinum, is the least reductive oxide. Hydrogen uptake exceeds the amount of platinum by a factor of 5, and no reduction is seen without platinum. This means hydrogen reduces only locally around the platinum structural changes, in line with previous studies showing that hydrogen spillover can occur for Pt/Al_2O_3 systems only to a minimal extent, if at all.[15,30]

Iron oxide, ceria, and titania showed interesting behavior in the presence of platinum. The TPR behavior of titania was recently studied in detail.[7] The hydrogen uptake behavior strongly depends on the hydrogen pressure used for reduction. For example, under 1 bar of hydrogen, anatase will transform into rutile at 900 K. Therefore, the iron oxide and ceria samples were further investigated with in-situ high-resolution X-ray diffraction (XRD) using synchrotron radiation of 36.6 keV. The heating rate was decreased compared to the hydrogen uptake measurements to 5 K min^{-1} to increase the temperature resolution of the experiment.

Figure 3a shows the evolution of the diffraction patterns of the iron oxide sample across selected temperatures. With increasing temperature, the initial reflections diminished, and new ones appeared. This observation evidences the phase transition, which was assumed from the high level of hydrogen consumption measured during the hydrogen uptake experiments. The final phase, which was present by the end of the diffraction experiment, was metallic bcc iron. However, a remaining 0.5% of Fe_3O_4 was also observed for platinum−iron oxide. The data were fitted using sequential Rietveld refinement. The resulting phase quantification (Figure 3b) shows the sequential reduction of Fe_2O_3 to Fe_3O_4 to Fe^0 for both samples. There are distinct differences between the two samples. In line with the previous observation (Figure 1), the platinum-containing iron oxide was reduced at a lower temperature (523 K vs 580 K). The difference in reduction temperature for the two samples was smaller than in the hydrogen uptake experiments due to the slower heating ramp in the diffraction experiment.[31] After Fe_3O_4 reached the

https://doi.org/10.1021/acs.jpcc.2c05478
J. Phys. Chem. C 2022, 126, 17589−17597

maximum concentration, metallic iron started forming. The iron formation occurred at similar temperatures (670 K) for both samples. Also, the temperature at which all iron oxide was converted into metallic iron was the same for both samples (790 K). Figure 3c shows the oxygen loss per temperature unit calculated from the phase fraction. These data can be compared to the TPR profiles in Figure 1a. The slower heating rate and higher gas hourly space velocity in the diffraction experiment lead to the complete reduction, while in the hydrogen uptake experiment (Figures 1 and 2), around 20% of the total accessible oxygen was removed by hydrogen. The XRD results show that the incomplete uptake observed in Figure 1 is purely due to kinetics, and a complete reduction is possible within the temperature and hydrogen pressure range. However, the shape of the TPR profile was very similar. Platinum mainly influences the initial reduction from Fe_2O_3 to Fe_3O_4. The reduction of Fe_3O_4 and the further reduction kinetics are independent of the platinum.

A deeper analysis revealed relevant differences, notably that together with the formation of metallic iron a small fraction of FeO (around 3%) was only formed when platinum was absent (Figure 3b). More remarkable are the particle size changes of the sample. The initial Fe_2O_3 particle size of the platinum-free sample was larger (around 1.7 μm) than the platinum-containing sample (0.3 μm). Even though the iron oxide was calcined before at higher temperatures (874 K), the platinum impregnation treatment, including calcination at lower temperatures (623 K), led to a restructuring of the iron oxide. Potentially, dissolution in the aqueous phase during impregnation strongly contributed to this process. In both cases, the reduction of Fe_2O_3 leads to the formation of Fe_3O_4 particles of much smaller domain size but similar for both samples (35 and 45 nm). The temperature at which the nucleation of *bcc* metallic iron occurs and at which it is fully formed is the same for both samples. The platinum has a smaller impact at higher temperatures, either because the hydrogen coverage is lower at higher temperatures, the thermodynamics of iron oxide reduction determines this step, or in both samples the rate-limiting step for the reduction is the same. Under the conditions in the reactor with a very high hydrogen-to-water ratio, metallic iron formation should be thermodynamically possible at lower temperatures.[32,33] Therefore, the reduction of metallic iron is dominated by the same rate-limiting step. The size evolution of the formed iron, however, is remarkably different for the two samples. The presence of platinum limited the crystal growth of bcc iron and allowed only 250 nm crystals that otherwise, upon the absence of platinum, reached beyond 1 μm size. This size difference indicates different reduction mechanisms. One potential explanation for this observation is that finely distributed platinum across the surface serves as nucleation sites, leading to a much higher number of nuclei, and, finally, smaller crystals. In the absence of platinum, nucleation of the iron phase occurs at fewer surface defects and favors crystal growth. Consequently, platinum significantly influenced the transformation of the catalyst during the reduction in hydrogen.

Figures 4a and b show the recorded diffraction patterns of Pt/CeO_2 and platinum-free ceria, respectively. None of the patterns indicate that a phase change occurred. All ceria reflections showed a shift to lower angles. In addition, the reflections of both samples became sharper. A consequent Rietveld refinement showed the evolution of the particle size (Figure 4c). Also, the platinum deposition treatment induced a change in particle size for ceria. However, in contrast to iron oxide, the platinum deposition caused an increase in ceria crystal size (from 3.7 to 4.9 nm). During the TPR up to 573 K, the ceria crystal size slightly shrunk (Figures 4c and d) by 0.8 and 0.9 Å for the loaded and unloaded Pt, respectively. This shrinkage corresponds to less than a unit cell loss. It may be due to the interaction of hydrogen with the surface. Indeed, for both samples, the two shrinkage events at 373 and 490 K coincide with the first measured hydrogen uptake (inset in Figure 4d). Beyond 573 K, both samples started to sinter. By the end of the experiment, both ceria samples reached similar particle sizes of 6.5 and 7.0 nm. Given these similarities in final size and growth-inducing temperature, platinum's presence did not significantly influence the sintering behavior under hydrogen. Since the ceria was initially calcined at 873 K, the sintering observed was induced by hydrogen.

Much larger differences were seen in the lattice parameter changes (Figure 4e). The ceria lattice parameter of Pt/CeO_2 increased sharply at 473 K. Then, the parameter plateaued and continued to increase at 773 K until the end of the experiment. The pure ceria sample behaved differently. Initially, the lattice parameter was larger than that of the platinum-containing ceria. It may be a strain effect on smaller grains packed in the packed catalyst bed. Upon increasing the temperature, there was no sudden increase in the lattice parameter, and the unit cell started to expand at a higher temperature (573 K). The lattice expansion exceeded that expected by a calculated linear thermal expansion (Figure 4e). The increase in the lattice parameter beyond thermal expansion can arise from two origins: the formation of larger Ce^{3+} ions (either by incorporating hydrogen into the ceria lattice or by oxygen removal from the lattice) or the incorporation of platinum into the ceria lattice.

Given that both samples arrive at the same final lattice parameter, the latter origin is unlikely. Lattice expansion was reported previously for bare ceria in hydrogen to occur above 600 K, which agrees with our observation.[34−36] Also, it was calculated that incorporating hydrogen into the ceria lattice to a stoichiometry of HCe_2O_4 results in a lattice parameter expansion of 1.5%.[37] Hydrogen incorporation is potentially reversible in a TPR experiment if hydrogen is released from the crystal lattice.[7,34] Oxygen removal is nonreversible during a TPR. Both effects potentially contribute to the observed process. The first derivative of the lattice parameter (corrected by the linear thermal expansion, Figure 4f) is directly proportional to the hydrogen uptake measured in Figure 1. The trend in the derivative of the lattice parameter resembles the uptake curve for both samples. For Pt/CeO_2, it was negative after the initial uptake (490−760 K). This shrinkage in the lattice parameter hints at the release of hydrogen from the ceria lattice. Adsorbed hydrogen will become less stable at higher temperatures and can desorb via reversible spillover.[38]

Since a change of the whole ceria bulk structure was seen at much lower temperatures for Pt/CeO_2, it is evident that the spillover process was not limited to a surface process. Most likely, the exchange of oxygen and cerium ions between the bulk and surface[39] and the migration of hydrogen into the lattice contribute to spreading the spillover throughout the sample. However, in the case of ceria, the final structure appears comparable to the platinum-free and -containing sample.

https://doi.org/10.1021/acs.jpcc.2c05478
J. Phys. Chem. C 2022, 126, 17589−17597

Scheme 1. Schematic Consequences of Hydrogen Interaction with Iron Oxide, Ceria, and Titania[a]

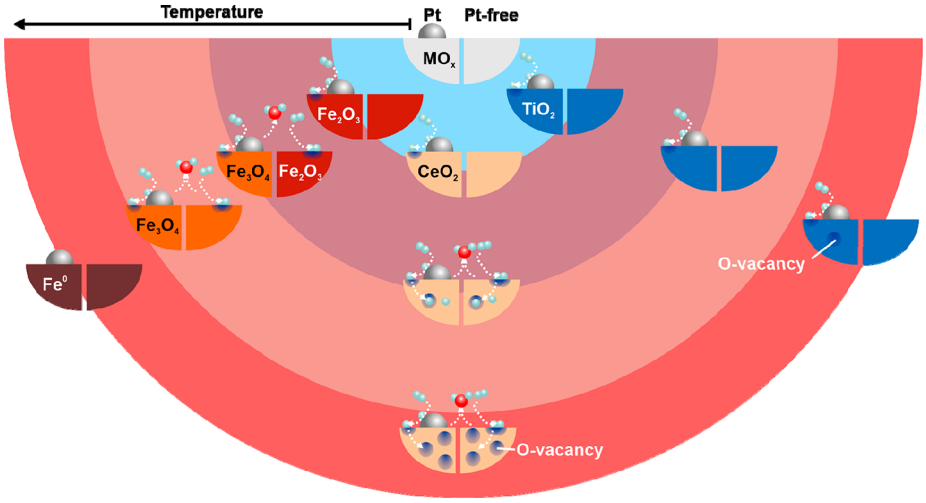

[a]The difference in hydrogen interaction for platinum-free and -containing samples is illustrated for the studied iron oxide, ceria, and titania. Iron oxide subsequently undergoes a phase transition to metallic iron. Ceria is taking up hydrogen, resulting in a change of the bulk lattice parameter. Lastly, titania only interacts with hydrogen in the presence of platinum (MO_x = metal oxide).

DISCUSSION

Even though the term reducibility is broadly used in the literature to describe the properties of oxides, there is not a single definition of the term reducibility.[28,41−43] Consequently, systematic studies like the present one are needed to elucidate aspects of reducibility and to broaden the understanding of this term. The detailed diffraction study of iron oxide and ceria and the TPR results for titania, zirconia, and alumina put these results into perspective. It is common to compare TPR studies of oxides with the same weight loading of, e.g., platinum.[22,44] In such studies, the different platinum surface density leads to deviating platinum structures.[20] In the present work, the comparison of oxide materials with the same surface loading of platinum allows in comparison to other studies direct quantitative evaluation of different behavior. For iron oxide, ceria, and titania, the major findings of this work are schematically depicted in Scheme 1, which highlights the diverse nature of hydrogen interaction with platinum−metal oxide catalysts.[13] Iron oxide has the lowest uptake temperature for hydrogen in the presence of platinum via spillover and is an excellent hydrogenation catalyst for aromatic nitrocompounds.[45] However, easily induced phase transition may be an unwanted effect in catalysis since it may corrupt the catalyst's lifetime. Furthermore, this low reduction temperature explains the origin of the very often reported encapsulation of the noble metal with iron oxide during reduction or reaction, the so-called classical strong metal−support interaction.[46−51]

Distinctively different from iron oxide are the other studied oxides. None of them undergo a crystal phase transformation. However, the XRD study on ceria revealed relevant details in the ceria structure. There is a temperature dependence of the hydrogen interaction. First, the ceria particles shrink, which suggests a surface reduction. This was also indicated by XPS depth profile measurements of a Pt/CeO_2 catalyst in hydrogen at 403 K, which saw an enriched concentration of Ce^{3+} at the surface.[52] Then, a substantial change in the lattice parameter occurred as soon as more pronounced hydrogen uptake occurred. Other work also suggested that hydrogen diffusion into the bulk occurs.[36,37] The differences in hydrogen uptake for ceria to titania are very interesting. Both oxides are considered as prominent reducible supports, and therefore, the behavior is assumed to be similar.[41] By direct comparison within one study it is shown that ceria can activate hydrogen on its own,[34,53] while for titania, platinum is required. Consequently, pure ceria can be used as a hydrogenation catalyst at elevated temperature,[54,55] and titania is merely a support for hydrogenation reactions and does not act on its own.[56,57] As soon as platinum is added, the uptake starts at lower temperatures. Consequently, hydrogen spillover readily occurs over Pt/TiO_2.[7] Even though the studied ceria and titania materials had comparable surface areas, the total hydrogen uptake for ceria was much higher. Therefore, hydrogen spillover in Pt/TiO_2 potentially remains mainly a surface process at temperatures below 673 K at low hydrogen pressures.[7] This limitation to a surface process is even more pronounced for zirconia. Here, normalization by surface area shows that the hydrogen uptake is comparable to titania. Nevertheless, the total uptake was relatively small. Using the stable zirconia for catalysis involving hydrogen spillover appears feasible.[58−60]

In a catalytic process that also contains oxidant as a catalytic reagent besides hydrogen, this oxidant can counteract the observed reduction processes, and therefore, the reduction may not proceed to such a deep level.[4,6] Moreover, the counterplay of hydrogen reduction and the following oxidation can induce dynamics at the platinum metal oxide interface, which would not occur in a purely reducing environment.[61]

CONCLUSION

In summary, the systematic study of the temperature-programmed hydrogen interaction showed that the fate of hydrogen and the consequences for the oxide structure are very different for different reducible oxides. The extent of phase transformation (which occurs for iron oxide), bulk reduction (ceria), and surface reduction (iron oxide > ceria > titania > zirconia > alumina) is oxide dependent. The addition of platinum reduces the temperature of hydrogen uptake and enhances the interaction in all metal oxides. Platinum acts as a hydrogen dissociative adsorption site and alters the oxide structure via hydrogen spillover. Assuming directly comparable

https://doi.org/10.1021/acs.jpcc.2c05478
J. Phys. Chem. C 2022, 126, 17589−17597

pathways of hydrogen spillover for all reducible metals results in an underestimation of this highly complex behavior.

■ ASSOCIATED CONTENT

Supporting Information

The Supporting Information is available free of charge at https://pubs.acs.org/doi/10.1021/acs.jpcc.2c05478.

XRD data and the fits of the in situ diffraction of the ceria and iron oxide samples (PDF)

■ AUTHOR INFORMATION

Corresponding Authors

Arik Beck − *Institute for Chemistry and Bioengineering, ETH Zurich, 8093 Zürich, Switzerland;* orcid.org/0000-0001-5267-3141; Email: arik.beck@chem.ethz.ch

Jeroen A. van Bokhoven − *Institute for Chemistry and Bioengineering, ETH Zurich, 8093 Zürich, Switzerland; Laboratory for Catalysis and Sustainable Chemistry, Paul Scherrer Institute, 5232 Villigen, Switzerland;* orcid.org/0000-0002-4166-2284; Email: jeroen.vanbokhoven@chem.ethz.ch

Authors

Przemyslaw Rzepka − *Institute for Chemistry and Bioengineering, ETH Zurich, 8093 Zürich, Switzerland; Laboratory for Catalysis and Sustainable Chemistry, Paul Scherrer Institute, 5232 Villigen, Switzerland;* orcid.org/0000-0003-3185-3535

Kenneth P. Marshall − *The Swiss-Norwegian Beamlines (SNBL) at ESRF, BP 220, Grenoble 38043, France*

Dragos Stoian − *The Swiss-Norwegian Beamlines (SNBL) at ESRF, BP 220, Grenoble 38043, France;* orcid.org/0000-0002-2436-6483

Marc G. Willinger − *TUM Department of Chemistry, Technical University of Munich, 85748 Garching, Germany;* orcid.org/0000-0002-9996-7953

Complete contact information is available at: https://pubs.acs.org/10.1021/acs.jpcc.2c05478

Author Contributions

A.B. and P.R. performed the experiments. A.B. analyzed the data. P.R. performed refinement of the XRD data. A.B., P.R., K.M., and D.S. performed the synchrotron experiments. A.B., M.G.W., and J.A.v.B. conceptualized and planned the study. J.A.v.B. provided funding for the work.

Notes

The authors declare no competing financial interest.

■ ACKNOWLEDGMENTS

Part of this work was performed at the European Synchrotron Research Facility (ESRF). We thank the Swiss Norwegian Beamlines (SNBL), specifically BM31, for access to synchrotron radiation (Proposal No. ch6283). A.B. and J.A.v.B. acknowledge the SNSF project 200021_178943. We thank Hannes Frey, Xiansheng Li, and Chiara Pischetola for their support during the beamtime.

■ REFERENCES

(1) Vilé, G.; Bridier, B.; Wichert, J.; Pérez-Ramírez, J. Ceria in Hydrogenation Catalysis: High Selectivity in the Conversion of Alkynes to Olefins. *Angew. Chemie - Int. Ed.* **2012**, *51* (34), 8620−8623.

(2) Liu, L.; Corma, A. Metal Catalysts for Heterogeneous Catalysis: From Single Atoms to Nanoclusters and Nanoparticles. *Chem. Rev.* **2018**, *118* (10), 4981−5079.

(3) van Deelen, T. W.; Hernández Mejía, C.; de Jong, K. P. Control of Metal-Support Interactions in Heterogeneous Catalysts to Enhance Activity and Selectivity. *Nat. Catal.* **2019**, *2* (11), 955−970.

(4) Beck, A.; Newton, M. A.; Zabilskiy, M.; Rzepka, P.; Willinger, M. G.; van Bokhoven, J. A. Drastic Events and Gradual Change Define the Structure of an Active Copper-Zinc-Alumina Catalyst for Methanol Synthesis. *Angew. Chemie - Int. Ed.* **2022**, *61*, e202200301 DOI: 10.1002/anie.202200301.

(5) Serna, P.; Boronat, M.; Corma, A. Tuning the Behavior of Au and Pt Catalysts for the Chemoselective Hydrogenation of Nitro-aromatic Compounds. *Top. Catal.* **2011**, *54* (5−7), 439−446.

(6) Beck, A.; Zabilskiy, M.; Newton, M. A.; Safonova, O.; Willinger, M. G.; van Bokhoven, J. A. Following the Structure of Copper-Zinc-Alumina across the Pressure Gap in Carbon Dioxide Hydrogenation. *Nat. Catal.* **2021**, *4* (6), 488−497.

(7) Beck, A.; Frey, H.; Becker, M.; Artiglia, L.; Willinger, M. G.; van Bokhoven, J. A. Influence of Hydrogen Pressure on the Structure of Platinum-Titania Catalysts. *J. Phys. Chem. C* **2021**, *125* (41), 22531−22538.

(8) Vilé, G.; Albani, D.; Almora-Barrios, N.; López, N.; Pérez-Ramírez, J. Advances in the Design of Nanostructured Catalysts for Selective Hydrogenation. *ChemCatChem.* **2016**, *8* (1), 21−33.

(9) Huang, W.; Ranke, W. Autocatalytic Partial Reduction of FeO(111) and Fe_3O_4(111) Films by Atomic Hydrogen. *Surf. Sci.* **2006**, *600* (4), 793−802.

(10) Borgschulte, A.; Gremaud, R.; Griessen, R. Interplay of Diffusion and Dissociation Mechanisms during Hydrogen Absorption in Metals. *Phys. Rev. B* **2008**, *78* (9), 094106.

(11) Lykhach, Y.; Staudt, T.; Vorokhta, M.; Skála, T.; Johánek, V.; Prince, K. C.; Matolín, V.; Libuda, J. Hydrogen Spillover Monitored by Resonant Photoemission Spectroscopy. *J. Catal.* **2012**, *285* (1), 6−9.

(12) Lykhach, Y.; Kubát, J.; Neitzel, A.; Tsud, N.; Vorokhta, M.; Skála, T.; Dvořák, F.; Kosto, Y.; Prince, K. C.; Matolín, V.; et al. Charge Transfer and Spillover Phenomena in Ceria-Supported Iridium Catalysts: A Model Study. *J. Chem. Phys.* **2019**, *151* (20), 204703.

(13) Shun, K.; Mori, K.; Masuda, S.; Hashimoto, N.; Hinuma, Y.; Kobayashi, H.; Yamashita, H. Revealing Hydrogen Spillover Pathways in Reducible Metal Oxides. *Chem. Sci.* **2022**, *13* (27), 8137−8147.

(14) Prins, R. Hydrogen Spillover. Facts and Fiction. *Chem. Rev.* **2012**, *112* (5), 2714−2738.

(15) Karim, W.; Spreafico, C.; Kleibert, A.; Gobrecht, J.; Vandevondele, J.; Ekinci, Y.; Van Bokhoven, J. A. Catalyst Support Effects on Hydrogen Spillover. *Nature* **2017**, *541* (7635), 68−71.

(16) Chupas, P. J.; Chapman, K. W.; Kurtz, C.; Hanson, J. C.; Lee, P. L.; Grey, C. P. A Versatile Sample-Environment Cell for Non-Ambient X-Ray Scattering Experiments. *J. Appl. Crystallogr.* **2008**, *41* (4), 822−824.

(17) Smeets, S. *Lines*; Zenodo, 2021. DOI: 10.5281/zenodo.4715908.

(18) Coelho, A. A. TOPAS and TOPAS-Academic: An Optimization Program Integrating Computer Algebra and Crystallographic Objects Written in C++. *J. Appl. Crystallogr.* **2018**, *51* (1), 210−218.

(19) Tanaka, I.; Oba, F.; Tatsumi, K.; Kunisu, M.; Nakano, M.; Adachi, H. Theoretical Formation Energy of Oxygen-Vacancies in Oxides. *Mater. Trans.* **2002**, *43* (7), 1426−1429.

(20) Maurer, F.; Beck, A.; Jelic, J.; Wang, W.; Mangold, S.; Stehle, M.; Wang, D.; Dolcet, P.; Gänzler, A. M.; Kübel, C.; et al. Surface Noble Metal Concentration on Ceria as a Key Descriptor for Efficient Catalytic CO Oxidation. *ACS Catal.* **2022**, *12*, 2473−2486.

(21) Huizinga, T.; Van Grondelle, J.; Prins, R. A Temperature Programmed Reduction Study of Pt on Al_2O_3 and TiO_2. *Appl. Catal.* **1984**, *10* (2), 199−213.

(22) Huizinga, T.; Prins, R. XPS Investigations of Al_2O_3 and TiO_2 supported Pt. *Stud. Surf. Sci. Catal.* **1982**, *11* (C), 11−17.

(23) Den Otter, G. J.; Dautzenberg, F. M. Metal-Support Interaction in Pt/Al_2O_3 Catalysts. *J. Catal.* **1978**, *53*, 116−125.
(24) Musso, J. C.; Parera, J. M. Adsorption and Spillover of Hydrogen on Al_2O_3 and Pt/Al_2O_3. *Appl. Catal.* **1987**, *30* (1), 81−90.
(25) Wang, J.; Li, G.; Li, Z.; Tang, C.; Feng, Z.; An, H.; Liu, H.; Liu, T.; Li, C. A Highly Selective and Stable ZnO-ZrO_2 Solid Solution Catalyst for CO_2 Hydrogenation to Methanol. *Sci. Adv.* **2017**, *3* (10), No. e1701290.
(26) Jabłońska, M. TPR Study and Catalytic Performance of Noble Metals Modified Al_2O_3, TiO_2 and ZrO_2 for Low-Temperature NH_3-SCO. *Catal. Commun.* **2015**, *70*, 66−71.
(27) Maity, S. K.; Rana, M. S.; Srinivas, B. N.; Bej, S. K.; Murali Dhar, G.; Prasada Rao, T. S. R. Characterization and Evaluation of ZrO_2 Supported Hydrotreating Catalysts. *J. Mol. Catal. A Chem.* **2000**, *153* (1−2), 121−127.
(28) Puigdollers, A. R.; Pacchioni, G. CO Oxidation on Au Nanoparticles Supported on ZrO_2: Role of Metal/Oxide Interface and Oxide Reducibility. *ChemCatChem.* **2017**, *9* (6), 1119−1127.
(29) Ruiz Puigdollers, A.; Schlexer, P.; Tosoni, S.; Pacchioni, G. Increasing Oxide Reducibility: The Role of Metal/Oxide Interfaces in the Formation of Oxygen Vacancies. *ACS Catal.* **2017**, *7* (10), 6493−6513.
(30) Prins, R.; Palfi, V. K.; Reiher, M. Hydrogen Spillover to Nonreducible Supports. *J. Phys. Chem. C* **2012**, *116* (27), 14274−14283.
(31) Knözinger, H. Temperature-Programmed Reduction and Oxidation. *Handbook of Heterogeneous Catalysis* **2008**, 1080−1096.
(32) Zhao, X.; Xu, N.; Li, X.; Gong, Y.; Huang, K. Solid Oxide Iron-Air Rechargeable Battery - A New Energy Storage Mechanism. *ECS Trans.* **2013**, *50* (45), 115−123.
(33) Pineau, A.; Kanari, N.; Gaballah, I. Kinetics of Reduction of Iron Oxides by H_2. *Thermochim. Acta* **2007**, *456* (2), 75−88.
(34) Clark, A. H.; Beyer, K. A.; Hayama, S.; Hyde, T. I.; Sankar, G. Unusual Redox Behavior of Ceria and Its Interaction with Hydrogen. *Chem. Mater.* **2019**, *31* (18), 7744−7751.
(35) Werner, K.; Weng, X.; Calaza, F.; Sterrer, M.; Kropp, T.; Paier, J.; Sauer, J.; Wilde, M.; Fukutani, K.; Shaikhutdinov, S.; et al. Toward an Understanding of Selective Alkyne Hydrogenation on Ceria: On the Impact of O Vacancies on H_2 Interaction with CeO_2(111). *J. Am. Chem. Soc.* **2017**, *139* (48), 17608−17616.
(36) Li, Z.; Werner, K.; Chen, L.; Jia, A.; Qian, K.; Zhong, J. Q.; You, R.; Wu, L.; Zhang, L.; Pan, H.; et al. Interaction of Hydrogen with Ceria: Hydroxylation, Reduction, and Hydride Formation on the Surface and in the Bulk. *Chem. - A Eur. J.* **2021**, *27* (16), 5268−5276.
(37) Sohlberg, K.; Pantelides, S. T.; Pennycook, S. J. Interactions of Hydrogen with CeO_2. *J. Am. Chem. Soc.* **2001**, *123* (27), 6609−6611.
(38) Rößner, F. Spillover Effects. In *Handbook of Heterogeneous Catalysis*; Wiley-VCH Verlag GmbH & Co. KGaA: Weinheim, Germany, 2008; pp 1574−1585.
(39) Perkins, C. L.; Henderson, M. A.; Peden, C. H. F.; Herman, G. S. Self-Diffusion in Ceria. *J. Vac. Sci. Technol. A Vacuum, Surfaces, Film.* **2001**, *19* (4), 1942−1946.
(40) Gupta, M. L.; Singh, S. Thermal Expansion of CeO2, Ho_2O_3, and Lu_2O_3 from 100° to 300 K by an X-Ray Method. *J. Am. Ceram. Soc.* **1970**, *53*, 663−665.
(41) Klissurski, D.; Dimitrova, R. Reducibility of Metal Oxides in Hydrogen and Strength of Oxygen Bond in Their Surface Layer. *Bull. Chem. Soc. Jpn.* **1990**, *63* (2), 590−591.
(42) Helali, Z.; Jedidi, A.; Syzgantseva, O. A.; Calatayud, M.; Minot, C. Scaling Reducibility of Metal Oxides. *Theor. Chem. Acc.* **2017**, *136* (9), 1−16.
(43) Rousseau, R.; Glezakou, V.-A.; Selloni, A. Theoretical Insights into the Surface Physics and Chemistry of Redox-Active Oxides. *Nat. Rev. Mater.* **2020**, *5* (6), 460−475.
(44) Rachmady, W.; Vannice, M. A. Acetic Acid Reduction by H_2 over Supported Pt Catalysts: A DRIFTS and TPD/TPR Study. *J. Catal.* **2002**, *207* (2), 317−330.
(45) Wang, Y.; Qin, R.; Wang, Y.; Ren, J.; Zhou, W.; Li, L.; Ming, J.; Zhang, W.; Fu, G.; Zheng, N. Chemoselective Hydrogenation of Nitroaromatics at the Nanoscale Iron(III)-OH-Platinum Interface. *Angew. Chem. - Int. Ed.* **2020**, *132* (31), 12836−12840.
(46) Liu, J.; Wang, L.; Okejiri, F.; Luo, J.; Zhao, J.; Zhang, P.; Liu, M.; Yang, S.; Zhang, Z.; Song, W.; et al. Deep Understanding of Strong Metal Interface Confinement: A Journey of Pd/FeO_x Catalysts. *ACS Catal.* **2020**, *10* (15), 8950−8959.
(47) Kast, P.; Friedrich, M.; Teschner, D.; Girgsdies, F.; Lunkenbein, T.; Naumann d'Alnoncourt, R.; Behrens, M.; Schlögl, R. CO Oxidation as a Test Reaction for Strong Metal-Support Interaction in Nanostructured Pd/FeO_x Powder Catalysts. *Appl. Catal. A Gen.* **2015**, *502* (1), 8−17.
(48) Zhu, M.; Tian, P.; Kurtz, R.; Lunkenbein, T.; Xu, J.; Schlögl, R.; Wachs, I. E.; Han, Y.-F. Strong Metal-Support Interactions between Copper and Iron Oxide during the High-Temperature Water-Gas Shift Reaction. *Angew. Chemie - Int. Ed.* **2019**, *58* (27), 9083−9087.
(49) Naumann D'Alnoncourt, R.; Friedrich, M.; Kunkes, E.; Rosenthal, D.; Girgsdies, F.; Zhang, B.; Shao, L.; Schuster, M.; Behrens, M.; Schlögl, R. Strong Metal-Support Interactions between Palladium and Iron Oxide and Their Effect on CO Oxidation. *J. Catal.* **2014**, *317*, 220−228.
(50) Yuan, X.; Pu, T.; Gu, M.; Zhu, M.; Xu, J. Strong Metal-Support Interactions between Nickel and Iron Oxide during CO_2 Hydrogenation. *ACS Catal.* **2021**, *11* (19), 11966−11972.
(51) Beck, A.; Huang, X.; Artiglia, L.; Zabilskiy, M.; Wang, X.; Rzepka, P.; Palagin, D.; Willinger, M.-G.; van Bokhoven, J. A. The Dynamics of Overlayer Formation on Catalyst Nanoparticles and Strong Metal-Support Interaction. *Nat. Commun.* **2020**, *11* (1), 3220.
(52) Kato, S.; Ammann, M.; Huthwelker, T.; Paun, C.; Lampimäki, M.; Lee, M.-T.; Rothensteiner, M.; van Bokhoven, J. A. Quantitative Depth Profiling of Ce^{3+} in Pt/CeO_2 by in Situ High-Energy XPS in a Hydrogen Atmosphere. *Phys. Chem. Chem. Phys.* **2015**, *17* (7), 5078−5083.
(53) Matz, O.; Calatayud, M. Breaking H2 with CeO_2: Effect of Surface Termination. *ACS Omega* **2018**, *3* (11), 16063−16073.
(54) Montini, T.; Melchionna, M.; Monai, M.; Fornasiero, P. Fundamentals and Catalytic Applications of CeO_2-Based Materials. *Chem. Rev.* **2016**, *116* (10), 5987−6041.
(55) Chang, K.; Zhang, H.; Cheng, M.; Lu, Q. Application of Ceria in CO_2 Conversion Catalysis. *ACS Catal.* **2020**, *10* (1), 613−631.
(56) Macino, M.; Barnes, A. J.; Althahban, S. M.; Qu, R.; Gibson, E. K.; Morgan, D. J.; Freakley, S. J.; Dimitratos, N.; Kiely, C. J.; Gao, X.; et al. Tuning of Catalytic Sites in Pt/TiO_2 Catalysts for the Chemoselective Hydrogenation of 3-Nitrostyrene. *Nat. Catal.* **2019**, *2* (10), 873−881.
(57) Corma, A.; Serna, P. Chemoselective Hydrogenation of Nitro Compounds with Supported Gold Catalysts. *Science* **2006**, *313* (5785), 332−334.
(58) Shishido, T.; Hattori, H. Spillover of Hydrogen over Zirconium Oxide Promoted by Sulfate Ion and Platinum. *Appl. Catal. A Gen.* **1996**, *146* (1), 157−164.
(59) Zabilskiy, M.; Ma, K.; Beck, A.; van Bokhoven, J. A. Methanol Synthesis over Cu/CeO_2-ZrO_2 Catalysts: The Key Role of Multiple Active Components. *Catal. Sci. Technol.* **2021**, *11* (1), 349−358.
(60) Chen, H.-Y. T.; Tosoni, S.; Pacchioni, G. Hydrogen Adsorption, Dissociation, and Spillover on Ru_{10} Clusters Supported on Anatase TiO_2 and Tetragonal ZrO_2 (101) Surfaces. *ACS Catal.* **2015**, *5* (9), 5486−5495.
(61) Frey, H.; Beck, A.; Huang, X.; van Bokhoven, J. A.; Willinger, M. G. Dynamic Interplay between Metal Nanoparticles and Oxide Support under Redox Conditions. *Science* **2022**, *376* (6596), 982−987.

https://doi.org/10.1021/acs.jpcc.2c05478
J. Phys. Chem. C 2022, 126, 17589−17597